

Abstract

Cold H^+ produced via charge exchange reactions between ring current ions and exospheric neutral hydrogen constitutes an additional source of cold plasma that further contributes to the plasmasphere and affects the plasma dynamics in the Earth's magnetosphere system; however, its production and associated effects on the plasmasphere dynamics have not been fully assessed and quantified. In this study, we perform numerical simulations mimicking an idealized 3-phase geomagnetic storm to investigate the role of heavy ion composition in the ring current (O^+ vs. N^+) and exospheric neutral hydrogen density in the production of cold H^+ via charge exchange reactions. It is found that ring current heavy ions produce more than 50% of the total cold H^+ via charge exchange reactions, and energetic N^+ is more efficient in producing cold H^+ via charge exchange reactions than O^+ . Furthermore, the density structure of the cold H^+ is highly dependent on the mass of the parent ion; that is, cold H^+ deriving from charge exchange reactions involving energetic O^+ with neutral hydrogen, populates the lower L-shells, while cold H^+ deriving from charge exchange reactions involving energetic N^+ with neutral hydrogen populate the higher L-shells. In addition, the density of cold H^+ produced via charge exchange reactions involving N^+ can be peak at values up to one order of magnitude larger than the local plasmaspheric density, suggesting that solely considering the supply of cold plasma from the ionosphere to the plasmasphere can lead to a significant underestimation of plasmasphere density.

1 Introduction

The terrestrial magnetospheric environment comprises of plasma populations with a wide range of energy profiles, spanning from the sub-eV and eV particles of the ionosphere and plasmasphere, up to the ultra-relativistic energies of the radiation belts particles. These diverse plasma populations coexist, interact, and exchange energy via a multitude of collisional and wave-particle interactions (e.g. Liemohn, 2006; Yu et al., 2019). The detection of cold plasma populations is significantly impacted by spacecraft charging and secondary-electron contamination, which make reliable measurements of the cold ion populations and their analysis difficult (e.g. Moore et al., 1997; Mozer et al., 2016; Genestreti et al., 2017; Gershman et al., 2017; Delzanno et al., 2021). The main source of the magnetospheric cold plasma is the ionosphere (Coley et al., 2003; Andersson et al., 2004; Haaland et al., 2015; Artemyev et al., 2020; Dandouras, 2021), which can also contribute to the hot component of the magnetospheric plasma (Chappell et al., 1987; Winglee, 2000; Huddleston et al., 2005; Glocer et al., 2009; Welling & Ridley, 2010; Brambles et al., 2010; Welling, André, et al., 2015). There is growing evidence that supports the hypothesis that magnetospheric cold plasma populations play critical roles in several important processes that drive the dynamics of the region (Winglee et al., 2002; Wiltberger et al., 2010; Brambles et al., 2011; Borovsky et al., 2013; Ouellette et al., 2013; Welling, Jordanova, et al., 2015; Trung et al., 2019; Delzanno et al., 2021). As a result, understanding the origin, properties, drivers, and impacts of cold plasma is a key to fully understanding the magnetosphere-ionosphere system.

While the cold-particle populations are sourcing a significant portion of the magnetospheric hot plasma, hot-particle populations can also become the source of cold plasma via charge exchange processes with regional neutral atoms (e.g. Borovsky et al., 2022). Due to the spatial overlap of the ring current with the Earth's neutral exosphere (Carruthers et al., 1976; Rairden et al., 1986), charge exchange processes between the low-energy exospheric neutral hydrogen atoms and the ring current ions, which allow for an energetic ion to pick up the orbital electron of a cold exospheric neutral hydrogen atom, lead to the formation of Energetic Neutral Atoms (ENAs) accompanied by low-energy H^+ . Therefore, the charge exchange process not only represents an important loss mechanism for the ring current energy density (Smith & Bewtra, 1978; Kistler et al., 1989; Liemohn et al., 1999; Liemohn & Kozyra, 2003, 2005; Ilie et al., 2013; Ilie & Liemohn, 2016), but also

69 leads to unstable hot-ion distributions in the ring current region (Cornwall, 1977; Thom-
 70 sen et al., 2011, 2017), and may also shorten the early-phase of the plasmaspheric refill-
 71 ing (Sojka & Wrenn, 1985; Su et al., 2001; Obana et al., 2010; Denton & Borovsky, 2014).
 72 While the density of exospheric neutral hydrogen decreases exponentially with increas-
 73 ing distance away from the Earth (e.g. Chamberlain, 1963; Ilie et al., 2013; Borovsky
 74 et al., 2022)), the details of cold H^+ production via charge exchange depend on the en-
 75 ergy profile, equatorial temperature distribution, convection drift pattern, and ion com-
 76 position of the hot plasma. Due to the different charge exchange cross sections for re-
 77 actions involving various ring current species with neutral hydrogen, changes in the re-
 78 gional ion composition can lead to changes in the cold H^+ population formed via the charge
 79 exchange interaction. Both numerical simulations and in situ measurements indicate that
 80 the ring current ion composition changes with the geomagnetic activity, and heavy ions
 81 (N^+ and O^+) can contribute significantly to the ring current number density during storm
 82 time (Hultqvist, 1979, 1982; Fu et al., 2001; Kozyra et al., 2002; Orsini, 2004; Zhao et
 83 al., 2015; Ilie et al., 2015; Kistler & Mouikis, 2016; Lee et al., 2021; James et al., 2021).

84 In this study, we assess the role of heavy ion composition of the ring current (and
 85 plasma sheet) in the production of cold H^+ via charge-exchange reactions. We present
 86 qualitative and quantitative estimations of the generation and time-evolution of these
 87 cold H^+ , with a special focus on those produced by the ring current N^+ and O^+ ions,
 88 based on numerical simulations using the Hot Electron-Ion Drift Integrator (HEIDI) model.
 89 In addition, the associated effects on the plasmaspheric refilling are also discussed.

90 2 Methodology

91 The HEIDI model is an inner magnetosphere kinetic drift model that solves the time-
 92 dependent, gyration- and bounce-averaged Boltzmann equation for the equatorial phase-
 93 space distribution function $F(t, \mathbf{r}_0, \mathbf{v}_0)$ of five ring current species (e^- , H^+ , He^+ , N^+ , O^+).
 94 The computational domain is defined by the surface of magnetic field minima between
 95 2 and 6.75 Earth radii, discretized uniformly both in the radial and azimuthal directions,
 96 and is capable of handling arbitrary electric and magnetic fields. The bounce-averaged
 97 kinetic equation solved is (Liemohn et al., 2004; Ilie et al., 2012):

$$\begin{aligned}
 \frac{\partial F}{\partial t} + \frac{1}{R_0^2} \frac{\partial}{\partial R_0} \left(R_0^2 \left\langle \frac{dR_0}{dt} \right\rangle F \right) + \frac{\partial}{\partial \phi_0} \left(\left\langle \frac{d\phi_0}{dt} \right\rangle F \right) + \frac{1}{\sqrt{W}} \frac{\partial}{\partial W} \left(\sqrt{W} \left\langle \frac{dW}{dt} \right\rangle F \right) \\
 + \frac{1}{h(\mu_0) \mu_0} \frac{\partial}{\partial \mu_0} \left(h(\mu_0) \mu_0 \left\langle \frac{d\mu_0}{dt} \right\rangle F \right) = \left\langle \frac{\delta F}{\delta t} \right\rangle_{collision} + \left\langle \frac{\delta F}{\delta t} \right\rangle_{source}
 \end{aligned} \quad (1)$$

99 Equation 1 describes the time-evolution of the phase-space distribution function
 100 at a certain location ($\mathbf{r}_0, \mathbf{v}_0$) within the configuration-velocity space, under the effect of
 101 drifts, energization, pitch-angle scattering, and various loss mechanisms. Ring current
 102 losses include Coulomb collisions, charge exchange reactions with the hydrogen exosphere,
 103 and precipitative losses to the upper atmosphere, all considering full pitch angle distri-
 104 butions. The five independent variables that constitute the equatorial phase-space dis-
 105 tribution function $F(t, \mathbf{r}_0, \mathbf{v}_0)$ are time t , radial distance on the magnetic equatorial plane
 106 R_0 , azimuth ϕ_0 , kinetic energy W , and the cosine of the equatorial pitch angle of each
 107 species $\mu_0 = \cos(\alpha_0)$. The size of the numerical grid was carefully determined to re-
 108 solve the features of interest, maintain numerical stability and accuracy, but also to op-
 109 timize the run-time of the simulation. The grid used in each mutually independent phase-
 110 space variable is as follows: 20s time step; 19 equally spaced radial grid points distributed
 111 from $2R_E$ to $6.5R_E$ geocentric distance ($\Delta R = 0.25R_E$); 24 equally spaced grid points
 112 in local time around the Earth ($\Delta \phi = \frac{\pi}{12} = 1\text{MLT}$); 42 geometrically spaced energy
 113 grid points from 10eV to 400keV, with the geometric factor of 1.26; and 71 equatorial
 114 pitch angle grid points from 90° to 0° , which corresponds to 0 to 1 in μ_0 and is more re-
 115 fined within loss cone angle. To calculate the bounce-averaged coefficients, HEIDI traces
 116 each individual field line whose equatorial intersection lies in the computation domain,

and employs a field-aligned grid that discretizes each field line (set to 101 points along the field line for this study, as described in Ilie et al. (2012)), along which the numerical integration is performed. The source term on the right hand side of Equation 1 is represented by the plasma sheet conditions on the nightside outer boundary of the simulation domain, using plasma sheet particle fluxes as the outer boundary condition.

The HEIDI model considers the loss of individual ring current ion species via charge exchange reactions with the neutral hydrogen exosphere, as described below:



where the H_{cold}^+ on the right hand side of each reaction denotes the cold protons produced via charge-exchange reactions between neutral hydrogen and ring current ions. At every time step, the charge exchange loss is reflected on the velocity distribution function $F_{\text{X}^+}(t, R_0, \phi_0, W, \mu_0)$, where $\text{X}^+ \in \{\text{H}^+, \text{He}^+, \text{O}^+, \text{N}^+\}$, as:

$$F_{\text{X}^+(\text{after})}(t, R_0, \phi_0, W, \mu_0) = F_{\text{X}^+(\text{before})}(t, R_0, \phi_0, W, \mu_0) \cdot \eta_{\text{X}^+(\text{CE})}(R_0, \phi_0, W, \mu_0) \quad (6)$$

where $F_{\text{X}^+(\text{before})}(t, R_0, \phi_0, W, \mu_0)$ and $F_{\text{X}^+(\text{after})}(t, R_0, \phi_0, W, \mu_0)$ represent the distribution function of ion X^+ before and after the charge exchange reaction took place, respectively. Furthermore, the term $\eta_{\text{X}^+(\text{CE})}(R_0, \phi_0, W, \mu_0)$ in Equation 6 represents the local charge exchange loss factor of ion species X^+ , calculated via:

$$\eta_{\text{X}^+(\text{CE})}(R_0, \phi_0, W, \mu_0) = \exp[-\sigma_{\text{X}^+}(W)v_{\text{X}^+}(W)\langle n_{\text{H}} \rangle(R_0, \phi_0, \mu_0)\Delta t] \quad (7)$$

where $\sigma_{\text{X}^+}(W)$ denotes the charge exchange cross section between species X^+ and exospheric neutral hydrogen (as a function of the kinetic energy W of the parent hot ion), $v_{\text{X}^+}(W)$ is the speed of X^+ , Δt is the timestep, and $\langle n_{\text{H}} \rangle(R_0, \phi_0, \mu_0)$ is the bounce-averaged neutral hydrogen density. Because the exosphere models are time independent, the local charge exchange loss factor $\eta_{\text{X}^+(\text{CE})}(R_0, \phi_0, W, \mu_0)$ is constant throughout the simulation.

The density distribution of the ring current species X^+ before and after the charge exchange process is obtained by evaluating the zeroth-order velocity moment of $F_{\text{X}^+(\text{before})}$ and $F_{\text{X}^+(\text{after})}$, respectively. The density of cold H^+ resulting from X^+ species, considering the contribution from the parent energetic ions of all energies and equatorial pitch-angles, is evaluated as:

$$\begin{aligned} n_{\text{H}_{\text{cold}}^+(\text{X}^+)}(t, R_0, \phi_0) &= n_{\text{X}^+(\text{before})}(t, R_0, \phi_0) - n_{\text{X}^+(\text{after})}(t, R_0, \phi_0) \\ &= \sum_k \sum_l F_{\text{X}^+(\text{before})}(t, R_0, \phi_0, W_k, \mu_{0l}) [1 - \eta_{\text{X}^+(\text{CE})}(R_0, \phi_0, W_k, \mu_{0l})] W_k \mu_{0l} \end{aligned} \quad (8)$$

where k and l denote the discrete energy and equatorial pitch-angle indexes of the parent species X^+ , respectively. The production of cold H^+ at each time step is accumulated, and the total density is obtained as the sum of the cold H^+ produced via charged exchange by all ring current ion species, as shown in Equation 9.

$$n_{\text{H}_{\text{cold}}^+(\text{total})} = n_{\text{H}_{\text{cold}}^+(\text{H}^+)} + n_{\text{H}_{\text{cold}}^+(\text{He}^+)} + n_{\text{H}_{\text{cold}}^+(\text{O}^+)} + n_{\text{H}_{\text{cold}}^+(\text{N}^+)} \quad (9)$$

The cold H^+ are assumed to be neither interacting with each other, nor participating in Coulomb interactions. The four $n_{\text{H}_{\text{cold}}^+}$ terms on the right hand side of Equation 9 denote the cold H^+ density resulted from each of the four ring current ion species (e.g. $n_{\text{H}_{\text{cold}}^+(\text{O}^+)}$ represents the cold H^+ density produced via charge exchange reactions of ring current O^+ with neutral exospheric hydrogen).

3 Simulation Setup

We investigated the effects of plasma composition on the generation and evolution of the cold H^+ population produced via charge exchange reactions with ring current ions, assuming idealized storm-like conditions and two neutral hydrogen exosphere models. In this study, we employed two typical exosphere neutral hydrogen models: 1) the spherically symmetric Rairden et al. (1986) model obtained via fitting the radial density profile with measurements of exospheric atomic hydrogen obtained from the ultraviolet imaging photometer carried on the high-altitude Dynamics Explorer 1 satellite (DE 1), and 2) the Hodges (1994) model obtained via 3D spherical harmonic expansion, which allows for asymmetry in the neutral hydrogen density distribution both on the dawn-dusk and day-night meridian. Several other exosphere density models exist (e.g. Zoennchen et al., 2011; Bailey & Gruntman, 2011, 2013; Zoennchen et al., 2015, 2022) and are included in the HEIDI model (Ilie et al., 2013); however, the formalism is based on the spherical harmonic expansion described in Hodges (1994), with the main difference that the expansion coefficients are either truncated or simplified. In the HEIDI model, the bounce-averaged neutral hydrogen density $\langle n_H \rangle$ is used to obtain the charge-exchange loss rate, as expressed in Equation 7. Panels (a) and (b) in Figure 1 show the bounce-averaged neutral hydrogen density (in log scale) imposed for energetic ions with an equatorial pitch-angle of 60° , using the Rairden et al. (1986) model and Hodges (1994) model, respectively. The pitch-angle of 60° is selected as example because it represents the set of energetic ions that travel further along the field line. The neutral hydrogen density predicted by both exosphere models decreases exponentially towards larger L-shells, and while the Rairden et al. (1986) model possesses spherical symmetry, the Hodges (1994) model does not. To highlight these differences, panel (c) in Figure 1 shows the percentage difference between the neutral densities predicted by the two models, indicating that the Hodges (1994) model predicts notably higher densities than that of the Rairden et al. (1986) model, with a significant intensification over the nightside. Specifically, the bounce-averaged neutral density of the Hodges (1994) model increases over 200% from the Rairden et al. (1986) model on the nightside for $L > 4$, while only 150% on the dayside.

The probability of occurrence of charge exchange reactions between ring current ions and exospheric neutral hydrogen depends on the energy of the incident energetic particles, the ambient exospheric neutral density, and the charge exchange cross section. The energy profile of the charge exchange cross section (in log scale) is shown in panel (d) of Figure 1 (Phaneuf et al., 1987). The weighted average charge exchange cross section of neutral hydrogen with energetic H^+ , O^+ and N^+ over all energies are $\sim 7 \times 10^{-21} \text{m}^{-2}$, $\sim 3 \times 10^{-20} \text{m}^{-2}$ and $\sim 1.0 \times 10^{-19} \text{m}^{-2}$, respectively. These differences in the charge exchange cross sections for different ion species with neutral hydrogen are due to the different ionization potentials of each species (Rapp & Francis, 1962). Please note that the average charge exchange cross sections of both N^+ and O^+ with the cold neutral hydrogen are notably higher than that of H^+ ; the cross section for the reaction involving N^+ is ~ 15 times larger than the cross section for the reaction involving H^+ , while the cross section for the reaction involving O^+ is ~ 4 times larger than the cross section for the reaction involving H^+ . This implies that energetic heavy ions are able to produce cold H^+ via charge exchange reactions with ambient neutral hydrogen more effectively compared with energetic H^+ on average, given the same local neutral density and energy distribution of parent ions. In addition, there are differences between the charge exchange cross section for reactions involving N^+ vs. O^+ and neutral hydrogen over the entire energy range; the cross section for the charge exchange reaction involving N^+ is on average 3.5 times larger than cross section for the charge exchange reaction involving O^+ , which implies that the specific composition of energetic heavy ions (O^+ vs. N^+) affects the amount of cold H^+ produced via charge exchange reactions in the inner magnetosphere. In this study, we focus on the production and evolution of cold H^+ produced via charge exchange involving different energetic heavy ions in the inner magnetosphere.

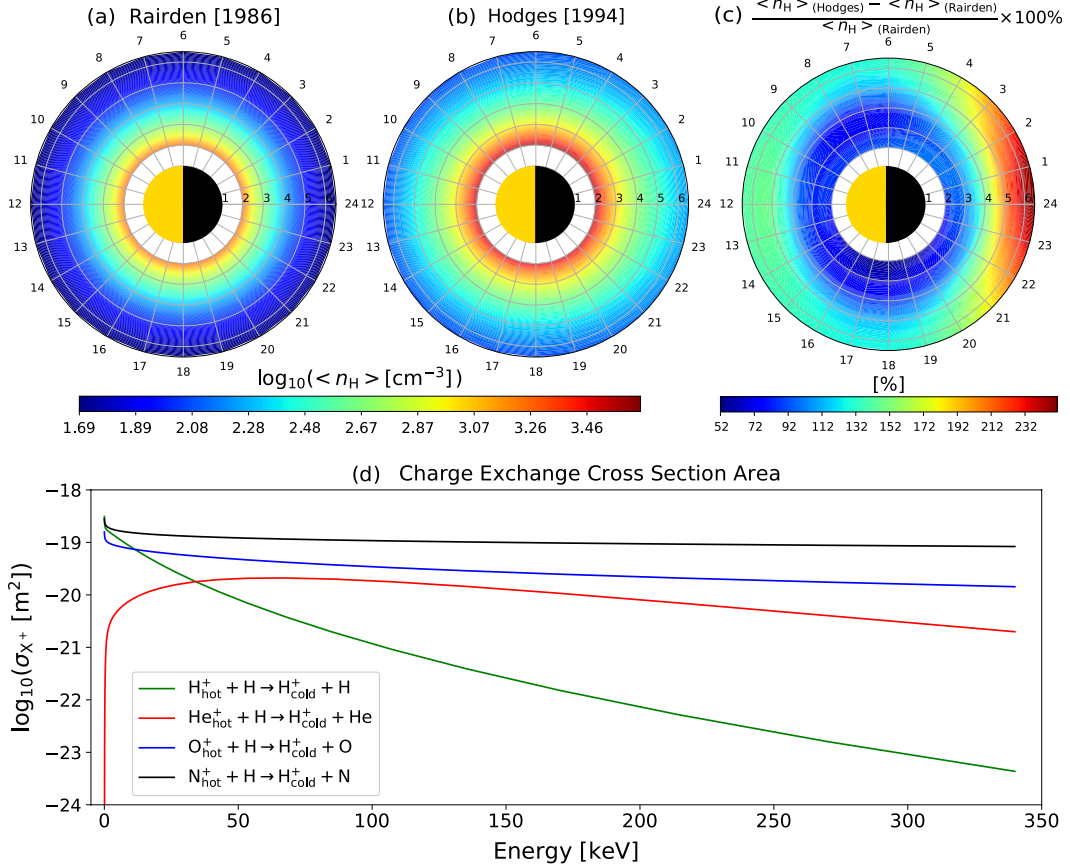


Figure 1. (a, b) Bounce-averaged neutral hydrogen density (on log scale) imposed to energetic ions with equatorial pitch-angle of 60° , using Rairden et al. (1986) model and Hodges (1994) model, respectively; (c) Percentage difference of the bounce-averaged exospheric neutral hydrogen density between the Rairden et al. (1986) model and Hodges (1994) model; (d) Charge exchange cross section vs. energy for reactions between energetic ions and the exospheric neutral hydrogen (see the plot label).

216 Numerical simulations are performed using a set of idealized parameters, designed
 217 to mimic a 3-phase geomagnetic storm that lasts for 72 hours, with a distinguishable quiet
 218 phase (the first 24 hours), main phase, and recovery phase (the last 24 hours). The vari-
 219 ations of the Kp index and nightside boundary total ion density are illustrated in panel
 220 (a) of both Figure 2 and Figure 3. Specifically, the Kp index and total ions density on
 221 the nightside boundary are set to 1 and 2cm^{-3} during both the quiet phase and recov-
 222 ery phase, and become 6 and 6cm^{-3} in the main phase, respectively. The simulation trans-
 223 its from the quiet phase into the main phase in 3 hours from $T = 24\text{h}$ to $T = 27\text{h}$,
 224 during which both the Kp index and the total plasma sheet density n_i on the outer bound-
 225 ary increase linearly to the main phase value, and transits from the main phase into the
 226 recovery phase in 3 hours from $T = 51\text{h}$ to $T = 54\text{h}$, during which the Kp index and
 227 total ion density n_i on the outer boundary drop linearly to the quiet phase values. The
 228 ring current ion composition is set up by splitting the total ion density n_i on the outer
 229 boundary into H^+ , He^+ and heavy ions ($\text{O}^+ + \text{N}^+$), via the Kp- and Ap-dependent sta-
 230 tistical relationships derived by Young et al. (1982). The convection electric field is pro-
 231 vided by the Kp-driven Volland-Stern's convection electric field model (Volland, 1973;
 232 Stern, 1975); and the dipolar magnetic field is strictly imposed across the computation
 233 domain throughout the entire simulation. In this study, we performed the 3-phase storm
 234 simulation under two independent cases of heavy ions composition: one where all heavy
 235 ions on the outer boundary are assumed to be O^+ , and the other where all heavy ions
 236 are assumed to be N^+ . The simulation results are discussed in Section 4.

237 4 Results and Discussion

238 The simulation results are presented and discussed in this section: Section 4.1 ex-
 239 plores the formation and evolution of the charge-exchange byproduct cold H^+ from the
 240 energetic heavy ions, with a primary focus on the storm phase and recovery phase, along
 241 with an investigation on the percentage contribution of energetic heavy ions to the cold
 242 H^+ over the total ring current ions; Section 4.2 compares the density of the byproduct
 243 cold H^+ via charge exchange with an activity dependent plasmasphere model, and dis-
 244 cusses the potential effects of the byproduct cold H^+ on the dynamics of the plasmas-
 245 phere.

246 4.1 Cold H^+ Production via Charge Exchange

247 Energetic heavy ions play a critical role in the production of the cold H^+ via charge
 248 exchange reactions, considering their notably higher average charge exchange cross sec-
 249 tions compared with energetic H^+ between neutral hydrogen, as showed in panel (d) of
 250 Figure 1 and discussed in Section 3. We first examine the production of cold H^+ that
 251 resulted from the charge exchange of O^+ and N^+ ions with exospheric neutral hydro-
 252 gen using the Rairden et al. (1986) exospheric density model, and assuming that the heavy
 253 ions injected on the nightside boundary are either 100% O^+ or 100% N^+ , respectively.
 254 These assumptions are designed to highlight the role of plasma sheet heavy ion compo-
 255 sition in the production of cold H^+ . Note that most previous studies considered O^+ the
 256 only heavy ion participating the ring current dynamics, and this corresponds to our case
 257 of 100% O^+ . Figure 2 shows the comparison between the ring current heavy ion den-
 258 sities and the associated cold H^+ resulting from the corresponding charge-exchange re-
 259 actions, extracted at four times within the numerical simulation ($T_1 = 27\text{h}$, $T_2 = 40\text{h}$,
 260 $T_3 = 51\text{h}$ and $T_4 = 72\text{h}$) indicated in panel (a). The following rows show the density
 261 of O^+ (row (b)) and N^+ (row (d)), and the associated cold H^+ (rows (c), (e)), as indi-
 262 cated by the highlighted red text at the bottom of each row.

263 At the beginning of the main phase ($T_1 = 27\text{h}$, the leftmost column), when both
 264 the convection strength and the flux on the nightside outer boundary are enhanced, we
 265 observe an increase in both O^+ and N^+ densities on the nightside centered on $L = 5$ shell,

266 as freshly injected particles are drifting westward while convecting into the lower L-shells
 267 (see leftmost column of rows (b) and (d)). During this time, there is no significant pro-
 268 duction of cold H^+ , which implies that the effects of charge-exchange reactions are not
 269 significant. This is due to the relatively low ring current ion densities, as well as to the
 270 fact that the peak density occurs at higher L-shells where the exospheric neutral den-
 271 sity is low.

272 At $T_2 = 40h$ during the storm main phase, we observe an enhancement in O^+ and
 273 N^+ densities in the evening sector (18 MLT — 0 MLT quadrant) between $L = 3$ and L
 274 $= 5$ shells, mostly due to the continuous supply of particles from the nightside bound-
 275 ary and strong Sunward convection. At this time, cold H^+ is being produced and accu-
 276 mulated close to the model inner boundary across the duskside around $L = 2.5$ shell (see
 277 rows (c) and (e)). This is due to the fact that the neutral density is exponentially de-
 278 creasing with distance away from the Earth, therefore the charge exchange reaction is
 279 most effective at low radial distances. In addition, the cold H^+ generated at higher L-
 280 shells (closer to the peak of ring current) are also drifting westward while convecting Earth-
 281 ward, leading to an accumulation of cold H^+ at lower L-shells.

282 At $T_3 = 51h$, which corresponds to the start of the recovery phase, the topology
 283 of the ring current becomes more symmetric. As energetic O^+ and N^+ drift around the
 284 simulation domain, they continue to undergo charge exchange reactions with the local
 285 exospheric neutral hydrogen, especially at lower L-shells where the density of neutral hy-
 286 drogen is high. Therefore, we observe a fast accumulation of cold H^+ accompanied by
 287 a faster decay of both O^+ and N^+ density at low L-shells. We observe that at the end
 288 of the simulation ($T_4 = 72h$), the charge exchange reactions led to a significant loss of
 289 energetic O^+ and N^+ from the ring current (see rows (b) and (d)). On the other hand,
 290 this ring current decay is associated with a significant production and accumulation of
 291 cold H^+ within $L = 4$ (rows (c) and (e)). The radial density profile of both the total en-
 292 ergetic ions and the associated charge-exchange byproduct cold H^+ along $MLT = 0$ (mid-
 293 night), captured at the end of the simulation ($T_4 = 72h$), are illustrated in panels (a)
 294 and (b) of Figure 4. It shows that the ring current ion density peaks between $L = 4$ and
 295 $L = 4.5$, while the associated byproduct cold H^+ density peaks around $L = 3.5$ (solid
 296 red and green) at the end of the simulation.

297 The evolution of the cold H^+ population associated with energetic O^+ and N^+ over
 298 the four time instances illustrated above, suggests that the production and topology of
 299 the cold ion population are closely controlled by the composition of ion plasma sheet along
 300 with the magnetospheric convection. The ion plasma sheet provides energetic ion pop-
 301 ulations that can be converted into the cold populations via charge exchange reactions,
 302 and the magnetospheric convection further transports the hot ion populations and drives
 303 them into lower L-shells where the exospheric neutral density is high. Therefore, it is the
 304 collective and accumulative effect of both ion plasma sheet composition and magneto-
 305 spheric convection that determines the abundance and topology of the cold populations
 306 associated with the ring current energetic ions.

307 Although energetic ring current O^+ and N^+ possess similar qualitative behaviors
 308 across the four time instances, significant quantitative differences exist. The energetic
 309 N^+ decays notably faster than O^+ during the recovery phase, as reflected by the den-
 310 sity of O^+ and N^+ showed in rows (b) and (d) of Figure 2. Those differences are also
 311 highlighted by the radial density profiles represented by the (either solid or dashed) red
 312 vs. green curves in panel (a) of Figure 4. The density of cold H^+ produced via charge
 313 exchange from N^+ with neutral hydrogen is notably higher than that produced in re-
 314 actions involving O^+ . This is due to the fact that the ring current N^+ undergoes more
 315 efficient charge-exchange loss than O^+ does, and has a shorter average ring current life-
 316 time, primarily due to the difference in charge exchange cross sections as showed in Fig-
 317 ure 1. The charge exchange cross section of hot N^+ with exospheric hydrogen is larger
 318 than that of O^+ across the entire considered energy range, inferring that the probabil-

319 ity of energetic N^+ undergoing charge exchange reactions with the local cold neutral hy-
 320 drogen is greater than that of energetic O^+ , given the same local density of cold neu-
 321 tral hydrogen. As a result, energetic N^+ is more efficient in producing cold H^+ . The ex-
 322 osphere density also plays a role on the decay rate of the energetic ions, as inferred by
 323 the difference between solid and dashed curves of the same color in panels (a) and (b)
 324 of Figure 4.

325 Next, we perform a quantitative assessment of the contribution of energetic O^+ and
 326 N^+ to the local production of cold H^+ generated by the charge exchange reactions be-
 327 tween the total ring current ions and neutral exosphere, for the two exospheric models
 328 described above. Figure 3 shows the fraction of $\frac{H^+_{\text{cold(heavy ions)}}}{H^+_{\text{cold(total)}}}$ (expressed in percentage)
 329 at the same four time moments discussed in Section 4.1. The black lines represent dif-
 330 ferent contour levels of the fraction $\frac{H^+_{\text{cold(heavy ions)}}}{H^+_{\text{cold(total)}}$, where $H^+_{\text{cold(heavy ions)}}$ denotes the cold
 331 H^+ derived from the charge exchange process involving a particular ring current heavy
 332 ion species (either O^+ or N^+) as indicated under the label of each row, along with the
 333 background exospheric neutral hydrogen model.

334 The contributions of cold H^+ associated with energetic O^+ and N^+ display distinct
 335 radial dependency, both qualitatively and quantitatively. At the end of the storm main
 336 phase ($T_3 = 51\text{h}$, the third column from the left), the contribution of energetic O^+ to
 337 the production of cold H^+ is less than 50% over the majority of the simulation domain,
 338 independent on the exosphere model employed, as shown by the region outside of the
 339 50% contribution contour in the third column from the left of rows (b) and (c); on the
 340 other hand, over 60% of cold H^+ is produced by charge exchange reactions of energetic
 341 N^+ with exospheric neutral hydrogen. This can be seen over a large region for $L > 3$ shell,
 342 independent of the exosphere model used, as shown by the region enclosed by the 60%
 343 contribution contour in the third column from the left of rows (d) and (e). At $T_4 = 72\text{h}$,
 344 the difference in cold H^+ contribution of O^+ or N^+ charge exchange reactions is signif-
 345 icant; the contribution of cold H^+ produced from energetic O^+ via charge exchange re-
 346 actions to the total cold H^+ population increases with decreasing distance from the Earth,
 347 with the 50% contribution contour centered at $L = 4$ for the simulation using the Rairden
 348 et al. (1986), whereas the same contour moves $1R_E$ outward for the simulation based on
 349 the Hodges (1994) exosphere model; in contrast, the contribution of the cold H^+ asso-
 350 ciated with energetic N^+ to the total cold H^+ population increases with increasing dis-
 351 tance from the Earth, independent of the ambient exospheric neutral density distribu-
 352 tion, as shown in the fourth column from the left of rows (d) and (e). The midnight (MLT
 353 = 0) radial profile of the cold H^+ contribution of both energetic O^+ and N^+ charge ex-
 354 change reactions with the neutral exosphere is presented in panel (c) of Figure 4. These
 355 simulations results suggest cold H^+ produced via charge exchange reactions with ring
 356 current O^+ is produced at lower L-shells, whereas production via charge exchange re-
 357 actions involving energetic N^+ is more efficient at larger L-shells (red curves vs. green
 358 curves). These differences imply that energetic O^+ ions have longer lifetimes and are more
 359 likely to convect into lower L-shells before they are lost via charge exchange; on the other
 360 hand, due to the high charge exchange cross section, energetic N^+ have shorter lifetimes
 361 and are lost via charge exchange reaction significantly faster, prohibiting their convec-
 362 tion deeper into the inner magnetosphere. Furthermore, the radial dependency of cold
 363 H^+ production via either O^+ or N^+ charge exchange reactions is independent of the ex-
 364 ospheric neutral hydrogen density, as seen in panel (c) of Figure 4.

365 The differences between the exospheric hydrogen densities predicted by the Rairden
 366 et al. (1986) and the Hodges (1994) models vary from $\sim 135\%$ to $\sim 250\%$ for $L \geq 3.5$ (see
 367 Figure 1). However, at the end of the recovery phase ($T_4 = 72\text{h}$), this significant dif-
 368 ference in neutral hydrogen density is only responsible for 1% change at best in the pro-
 369 duction of cold H^+ , both for reactions involving O^+ and N^+ . For instance, the average
 370 contribution of energetic O^+ to the production of cold H^+ increases from 47.7% to 49.2%,

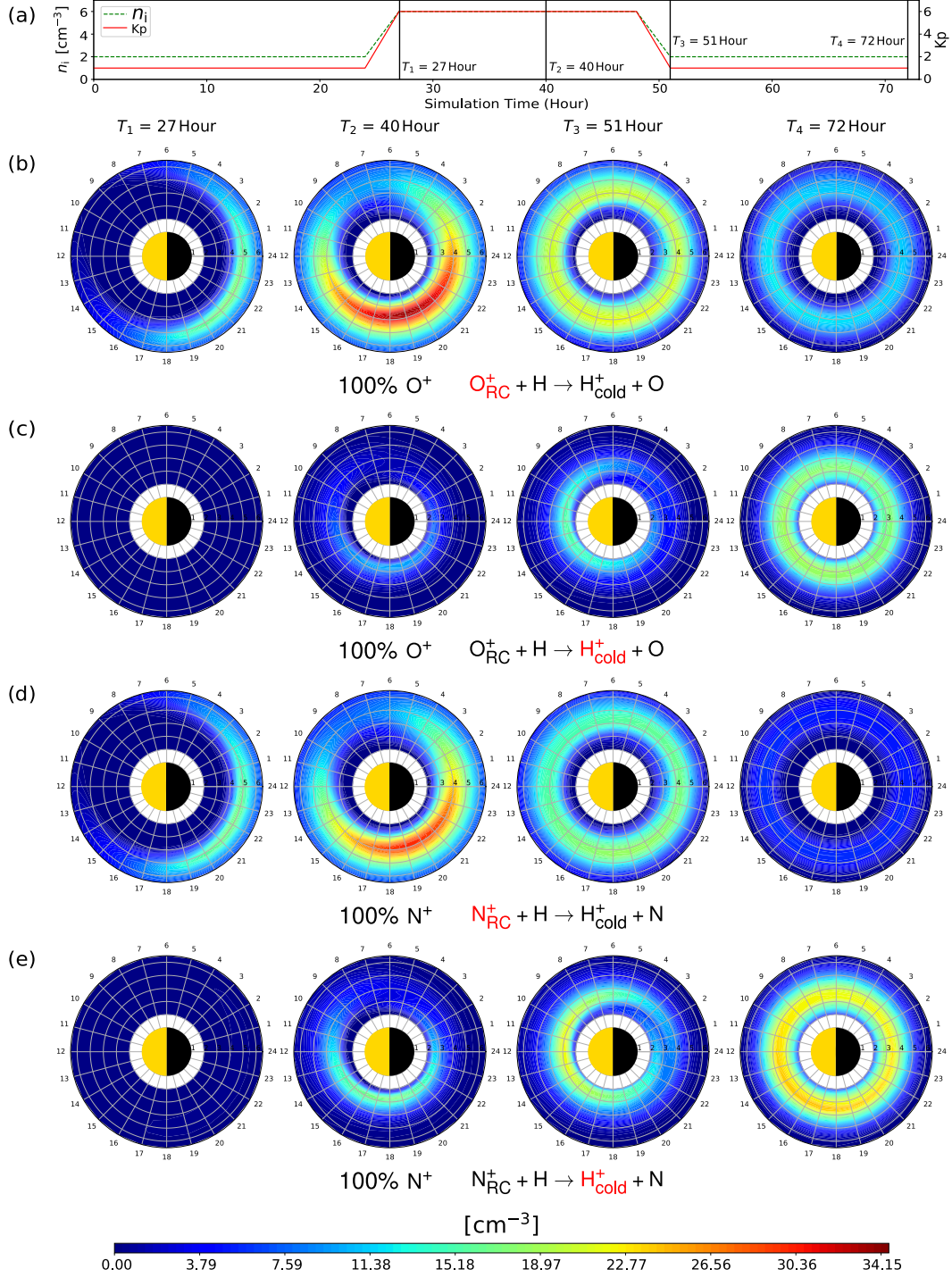


Figure 2. (a) Evolutionary tracks of the input parameters for the idealized storm simulations showing the Kp index (right y-axis, red line) and plasma sheet density on the nightside outer boundary (left y-axis, green line); (b, c, d, e) Plots showing the evolution of ring current heavy ions density and the associated charge-exchange byproduct cold H^+ at the four time instances, using the symmetric Rairden et al. (1986) model; (b, d) Ring current heavy ions density, assuming 100% O^+ and 100% N^+ ; (c, e) Charge-exchange byproduct cold H^+ density by the energetic heavy ions, assuming 100% O^+ and 100% N^+ .

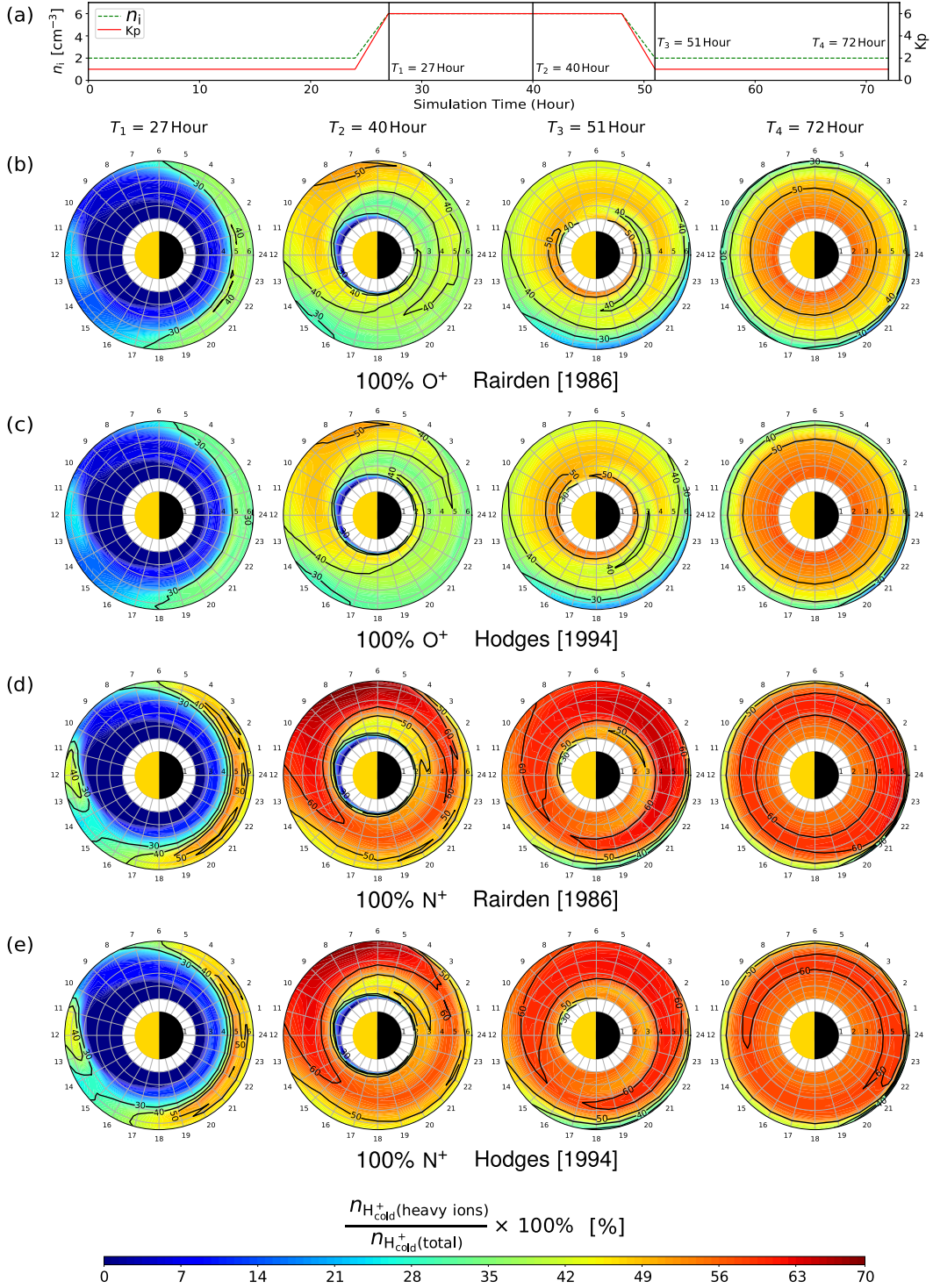


Figure 3. (a) Evolutionary tracks of the input parameters for the idealized storm simulations showing the Kp index (right y-axis, red line) and plasma sheet density on the nightside outer boundary (left y-axis, green line); (b, c, d, e) Plots showing the evolution of the cold H^+ density ratio (in %) between byproduct of the ring current heavy ions, and byproduct of the total ring current ions; (b, c) 100% O^+ using Rairden et al. (1986) model and Hodges (1994) model; (d, e) 100% N^+ using Rairden et al. (1986) model and Hodges (1994) model.

371 with an increase in the peak production fraction from 56.9% to 57.4%, as the exosphere
 372 model changes from the Rairden et al. (1986) to the Hodges (1994) model; however, the
 373 contribution of energetic N^+ to the production of cold H^+ is increasing by about 10%
 374 on average, as compared with the contribution of energetic O^+ for the same exospheric
 375 density distribution. Therefore, the production of cold H^+ is primarily determined by
 the plasma sheet composition, rather than the neutral exosphere density.

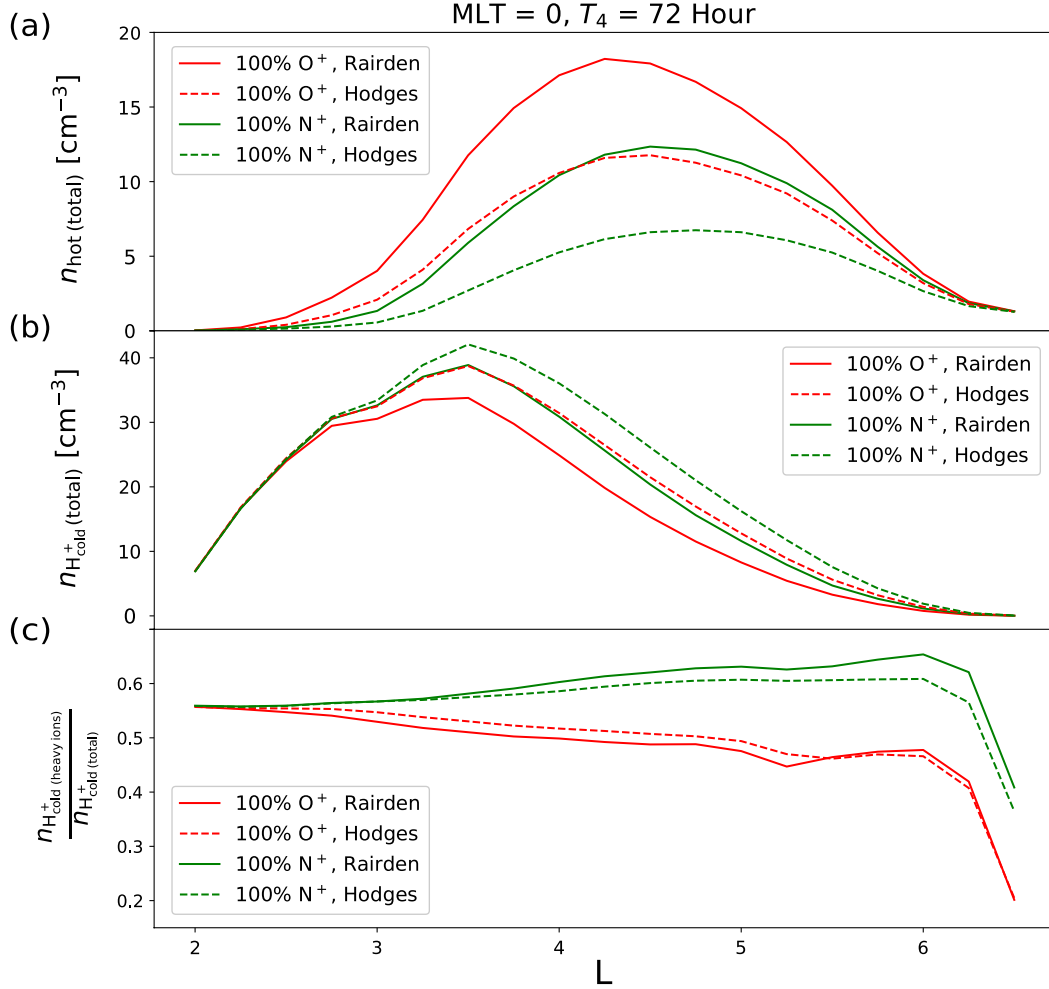


Figure 4. (a, b, c) Comparisons of radial profiles along MLT = 0 at the end of the simulation ($T_4 = 72$ h), between the two different heavy ions compositions of 100% O^+ (red) and 100% N^+ (green), using Rairden et al. (1986) model (solid) and Hodges (1994) model (dashed); (a) The radial density profile of the total energetic ions; (b) The radial density profile of the charge-exchange byproduct cold H^+ resulting from all energetic ions; (c) The radial profile of the cold H^+ contribution from the energetic heavy ions.

376

377

4.2 The Contribution of Cold H^+ to the Plasmasphere

378

379

380

381

Due to the spatial overlap between the plasmasphere and the ring current, the generation of cold H^+ via charge exchange can also affect the dynamics of the plasmasphere. To investigate these effects, we adopted the activity-dependent Dynamic Global Core Plasma Model (DGCPM) (Ober et al., 1997), included in the HEIDI model (Liemohn et al., 2005;

382 Ilie et al., 2012). DGCPM simulates the evolution of the low-energy plasma density by
 383 solving the mass continuity equation along convecting magnetic flux tubes for the to-
 384 tal cold ion content. The plasmaspheric density distribution (in log scale) at four dif-
 385 ferent time moments ($T_0 = 24\text{h}$, $T_3 = 51\text{h}$, $T'_3 = 58\text{h}$ and $T_4 = 72\text{h}$) are shown in row
 386 (b) of Figure 5. Please note that T_3 and T_4 are the same with the ones discussed in Sec-
 387 tion 4.1, while T_0 and T'_3 are two additional timestamps introduced in this section, as
 388 they are relevant in the context of the plasmasphere dynamics. At the end of the quiet
 389 phase ($T_0 = 24\text{h}$, the leftmost column), the distributions of plasmaspheric cold density
 390 is approximately symmetric around the Earth, with a slight dusk bulge. At the end of
 391 the storm main phase ($T_3 = 51\text{h}$, the second column from the left), the plasmasphere
 392 has been significantly eroded, with the plasmaspheric drainage plume extending from
 393 the afternoon sector (12 MLT — 18 MLT quadrant), and a well-defined nightside plasma-
 394 pause density gradient. The plasmasphere gradually refills during the recovery phase (51h
 395 $< T < 72\text{h}$), with the drainage plume rotating eastward and the cold plasma density re-
 396 covers.

397 The cold H^+ population produced via charge exchange reactions between ring cur-
 398 rent ions and neutral exospheric hydrogen also contributes to the overall plasmaspheric
 399 cold plasma density, therefore further affects its dynamics. Figure 6 shows the compar-
 400 ison of cold plasma as 10cm^{-3} (red) and 30cm^{-3} (blue) density contours, including (solid)
 401 and excluding (dashed) the contribution from cold H^+ populations formed via charge
 402 exchange reactions. At the beginning of the recovery phase ($T_3 = 51\text{h}$, the second col-
 403 umn from the left of rows (b) and (d), red solid contour vs. red dashed contour), inclu-
 404 sion of cold H^+ produced via charge exchange reactions involving energetic O^+ into the
 405 plasmaspheric population extends the 10cm^{-3} density contour at dawn from $L = 2.75$
 406 to $L = 4$, and those resulting from energetic N^+ further extends it to $L = 4.25$. At $T'_3 =$
 407 58h , inclusion of cold H^+ produced via charge exchange reactions involving energetic O^+
 408 into the plasmaspheric population extends the 10cm^{-3} density contour at dawn from L
 409 $= 3.25$ to $L = 4$, and those resulting from charge exchange reactions involving energetic
 410 N^+ further extends it to $L = 4.5$. This expansion of the cold plasma density during the
 411 early recovery phase implies that energetic heavy ions alone are able to produce cold H^+
 412 in amounts large enough to reshape the density distribution of the plasmasphere along
 413 with the plasmopause, especially during the early stage of the storm recovery phase. There-
 414 fore, the composition of the energetic heavy ions of the plasma sheet can affects the over-
 415 all spatial extent of the plasmasphere, as shown in row (c) with (e).

416 The expansion of the 10cm^{-3} plasmaphere density contour during the storm re-
 417 covery phase suggests that the local density of cold H^+ produced via charge exchange
 418 can be abundant compared with the local plasmasphere density, in the L-shells just greater
 419 the red dashed contours in Figure 6. This additional source of thermal H^+ can supply
 420 a significant portion of the plasmaspheric cold population, facilitating the plasmasphere
 421 refilling rate. Figure 7 shows the ratio (in log scale) between the cold H^+ density pro-
 422 duced by charge exchange reactions and the plasmaspheric density provided by Ober et
 423 al. (1997) model, revealing a broad region of high density ratio (~ 10) that lies on the
 424 nightside between $L = 3$ to $L = 5$ and $\text{MLT} = 20$ to $\text{MLT} = 7$ at the beginning of the
 425 recovery phase ($T_3 = 51\text{h}$, the second column from the left), which diminishes as the
 426 plasmasphere recovers. Comparison between the location of the 10cm^{-3} contour at the
 427 end of the quiet phase ($T_0 = 24\text{h}$) and the start of the recovery phase ($T_3 = 51\text{h}$), high-
 428 lights the presence of a plasmasphere density trough; here, the plasmaspheric cold plasma
 429 is significantly eroded during the storm main phase, and the most of the high-ratio re-
 430 gion, including the global ratio peak, is overlapping with the density trough. Specifically,
 431 the production of cold H^+ (row (e)) can be as much as 13.6 times the local plasmasphere
 432 cold density as predicted by the DGCPM model, assuming all the heavy ions are N^+ .
 433 Similarly, for the case when all the energetic heavy ions are O^+ , the local production of
 434 cold H^+ by total ring current ions (row (c)) can be as much as 10 times the plasmaspheric
 435 cold density predicted by the DGCPM model. Therefore, solely considering the cold plasma

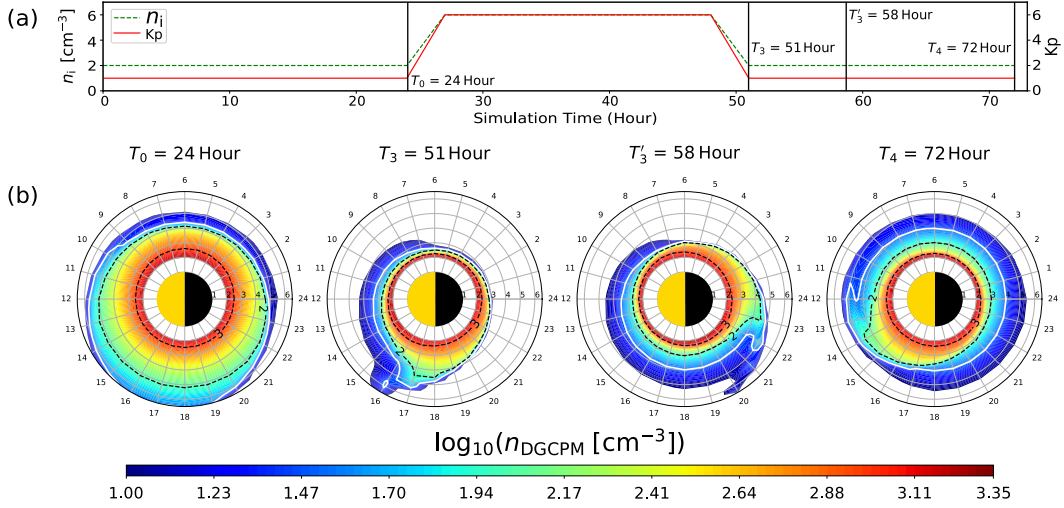


Figure 5. (a) Evolutionary tracks of the input parameters for the idealized storm simulations showing the Kp index (right y-axis, red line) and plasma sheet density on the nightside outer boundary (left y-axis, green line); (b) Plots showing the evolution of the plasmaspheric cold plasma density predicted by Ober et al. (1997) plasmasphere model (in log scale), with the white solid contour marks at constant density level of 30cm^{-3} .

supplemented from the ionosphere leads to an significant underestimation of plasmasphere density, especially in the density trough during the early state of the recovery phase.

5 Summary and Conclusions

In this study, we quantified the role of ion composition in the plasma sheet, together with the density of exospheric neutral hydrogen in the production and transport of cold H^+ via charge exchange reactions. The simulation results show that: (1) the production and topology of the cold H^+ population are closely controlled by the composition of plasma sheet and the strength of the magnetospheric convection; (2) the density distribution of the exosphere does not play a role in shaping the peak and overall topology of the cold H^+ density distribution, which is instead shown to be primarily determined by the composition of energetic heavy ions (O^+ and N^+); (3) the cold H^+ produced via charge exchange reactions can reshape the density distribution of the plasmasphere, and has the potential to enhance the early-stage plasmaspheric refilling rate by supplying an additional source to the plasmasphere density trough; (4) The density of cold H^+ produced via charge exchange reactions can be ~ 10 times greater than the local cold plasma supplied from the ionosphere in the plasmasphere density trough, therefore solely considering the supply of cold plasma from the ionosphere to the plasmasphere can lead to a significant underestimation of plasmasphere density, especially in the early recovery phase. (5) the cold H^+ deriving from charge exchange reactions involving energetic O^+ with neutral hydrogen, populate the inner L-shells, while the cold H^+ deriving from charge exchange reactions involving energetic N^+ with neutral hydrogen populate the larger L-shells.

Numerical simulations of ring current and plasmaspheric dynamics are performed under the assumption that the heavy ions supplied by the nightside plasma sheet are either O^+ or N^+ . Albeit idealized, these numerical experiments reveal several important physical factors and mechanisms with profound implications regarding the generation

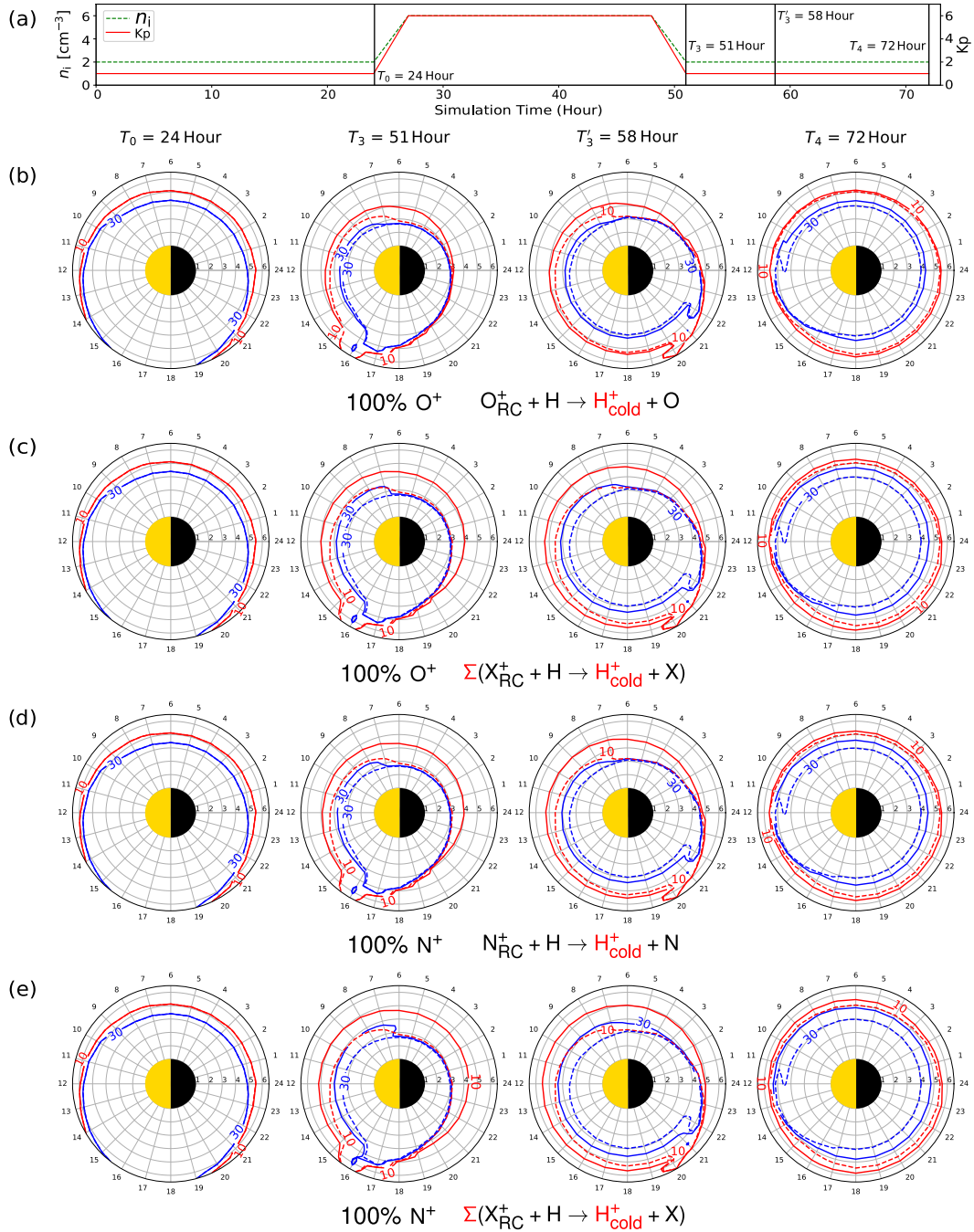


Figure 6. (a) Evolutionary tracks of the input parameters for the idealized storm simulations showing the Kp index (right y-axis, red line) and plasma sheet density on the nightside outer boundary (left y-axis, green line); (b, c, d, e) 10cm^{-3} (red) and 30cm^{-3} (blue) density contour levels of Ober et al. (1997) model (dashed) and the ones after considering the contribution from the charge-exchange byproduct cold H^+ populations (solid), using the symmetric Rairden et al. (1986) model; (b, d) Considering the byproduct cold H^+ that resulted from energetic heavy ions, assuming 100% O^+ and 100% N^+ ; (c, e) Considering the byproduct cold H^+ that resulted from all energetic ions, assuming 100% O^+ and 100% N^+ .

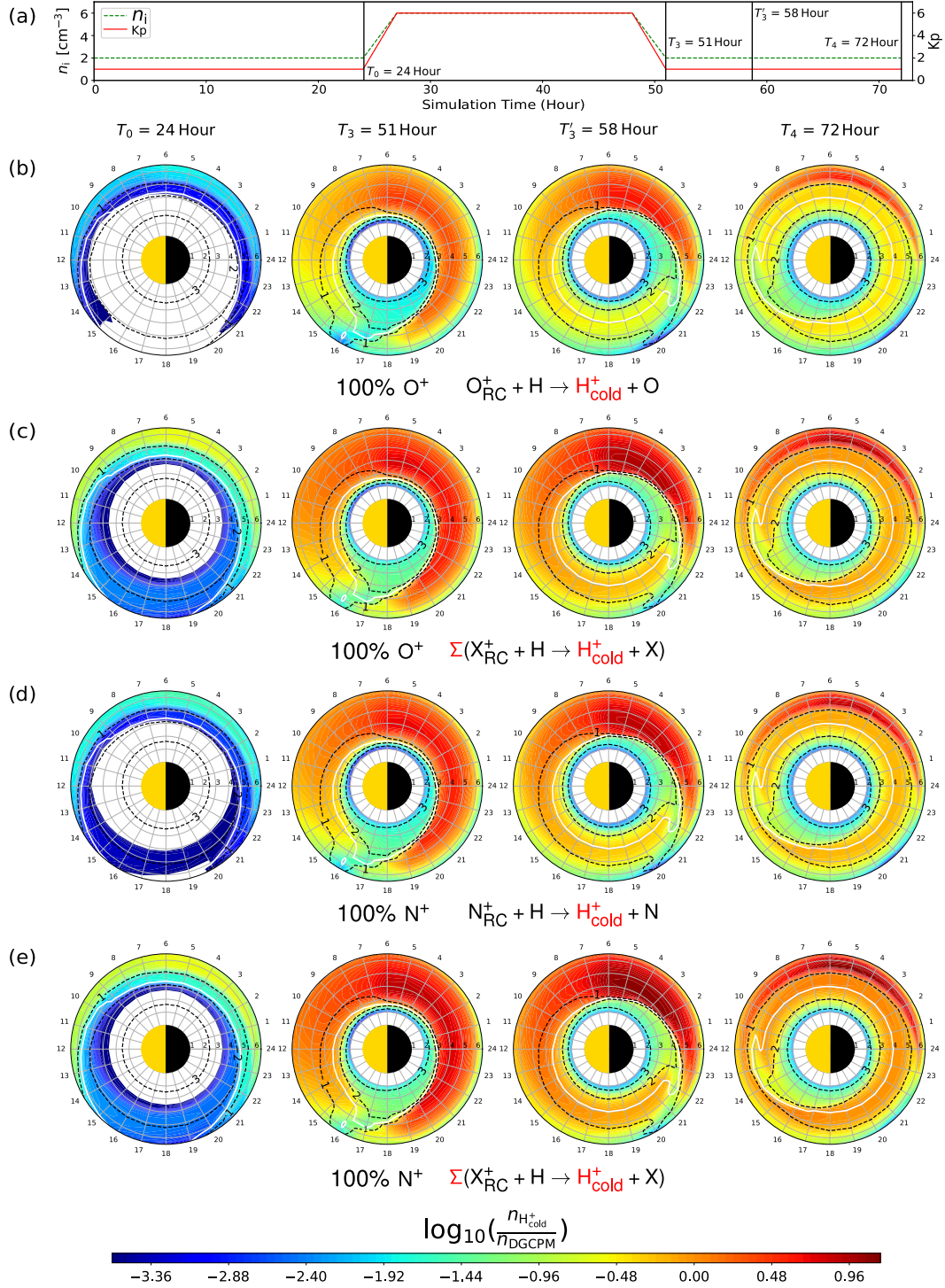


Figure 7. (a) Evolutionary tracks of the input parameters for the idealized storm simulations showing the Kp index (right y-axis, red line) and plasma sheet density on the nightside outer boundary (left y-axis, green line); (b, c, d, e) The density ratio (in log scale) between the charge-exchange byproduct cold H^+ highlighted by the red text at the bottom of each row, and the plasmaspheric cold plasma predicted by Ober et al. (1997) model. The black dashed contours represent the density levels of Ober et al. (1997) model (in log scale), and the white solid contour marks constant density level of 30cm^{-3} . The symmetric Rairden et al. (1986) model is used.

463 and evolution of the cold plasma populations, including the composition of the plasma
 464 sheet, the strength and nature of the magnetospheric convection, and the interplay be-
 465 tween the energetic ring current plasma, neutral atmosphere, and the plasmasphere. This
 466 study also infers that the cold H^+ generated via charge exchange reactions has the po-
 467 tential to significantly alters the local refilling of the plasmasphere during the early re-
 468 recovery phase.

469 Open Research

470 The HEIDI model has been included in the Space Weather Modeling Framework
 471 (SWMF), which is available for download at <http://csem.engin.umich.edu/tools/swmf>.
 472 The full set of simulation data is available at <https://doi.org/10.6084/m9.figshare.c.5979331.v1>.

473 Acknowledgments

474 Work at University of Illinois at Urbana-Champaign was performed with financial sup-
 475 port from the NASA grant N99066ZO, NASA grant 80NSSC20K1231, the NSF award
 476 1664078 and NSF CAREER award 1945573. Work at University of Michigan was per-
 477 formed with financial support from the NASA grants 80NSSC19K0077 and 80NSSC17K0015.
 478 Joseph E. Borovsky was supported by the NSF GEM Program via grant AGS-2027569.

479 References

- 480 Andersson, L., Peterson, W. K., & McBryde, K. M. (2004). Dynamic coordinates
 481 for auroral ion outflow. *Journal of Geophysical Research: Space Physics*,
 482 *109*(A8). Retrieved from [https://agupubs.onlinelibrary.wiley.com/doi/](https://agupubs.onlinelibrary.wiley.com/doi/abs/10.1029/2004JA010424)
 483 [abs/10.1029/2004JA010424](https://doi.org/10.1029/2004JA010424) doi: <https://doi.org/10.1029/2004JA010424>
- 484 Artemyev, A. V., Angelopoulos, V., Runov, A., & Zhang, X.-J. (2020). Iono-
 485 spheric outflow during the substorm growth phase: Themis observations
 486 of oxygen ions at the plasma sheet boundary. *Journal of Geophysical Re-*
 487 *search: Space Physics*, *125*(7), e2019JA027612. Retrieved from [https://](https://agupubs.onlinelibrary.wiley.com/doi/abs/10.1029/2019JA027612)
 488 [agupubs.onlinelibrary.wiley.com/doi/abs/10.1029/2019JA027612](https://doi.org/10.1029/2019JA027612)
 489 (e2019JA027612 10.1029/2019JA027612) doi: [https://doi.org/10.1029/](https://doi.org/10.1029/2019JA027612)
 490 [2019JA027612](https://doi.org/10.1029/2019JA027612)
- 491 Bailey, J., & Gruntman, M. (2011, September). Experimental study of exospheric
 492 hydrogen atom distributions by Lyman-alpha detectors on the TWINS mis-
 493 sion. *Journal of Geophysical Research (Space Physics)*, *116*(A15), A09302. doi:
 494 [10.1029/2011JA016531](https://doi.org/10.1029/2011JA016531)
- 495 Bailey, J., & Gruntman, M. (2013, September). Experimental Study of the Asym-
 496 metric Time Varying Exosphere by Lyman-alpha Detectors on the TWINS
 497 Mission. *European Planetary Science Congress 2013, held 8-13 September in*
 498 *London, UK. Online at: $\langle A href="http://meetings.copernicus.org/epsc2013" \rangle$*
 499 *$\langle A href="http://meetings.copernicus.org/epsc2013j/Aj, id.EPSC2013-861, 8, 861.$*
- 500 Borovsky, J. E., Denton, M. H., Denton, R. E., Jordanova, V. K., & Krall, J. (2013).
 501 Estimating the effects of ionospheric plasma on solar wind/magnetosphere
 502 coupling via mass loading of dayside reconnection: Ion-plasma-sheet oxy-
 503 gen, plasmaspheric drainage plumes, and the plasma cloak. *Journal of*
 504 *Geophysical Research: Space Physics*, *118*(9), 5695-5719. Retrieved from
 505 <https://agupubs.onlinelibrary.wiley.com/doi/abs/10.1002/jgra.50527>
 506 doi: <https://doi.org/10.1002/jgra.50527>
- 507 Borovsky, J. E., Liu, J., Ilie, R., & Liemohn, M. W. (2022). Charge-exchange
 508 byproduct cold protons in the earth's magnetosphere. *Frontiers in Astron-*
 509 *omy and Space Sciences*, *8*. Retrieved from [https://www.frontiersin.org/](https://www.frontiersin.org/article/10.3389/fspas.2021.785305)
 510 [article/10.3389/fspas.2021.785305](https://doi.org/10.3389/fspas.2021.785305) doi: [10.3389/fspas.2021.785305](https://doi.org/10.3389/fspas.2021.785305)
- 511 Brambles, O. J., Lotko, W., Damiano, P. A., Zhang, B., Wiltberger, M., & Lyon,

- 512 J. (2010). Effects of causally driven cusp outflow on the storm time
513 magnetosphere-ionosphere system using a multifluid global simulation. *Journal*
514 *of Geophysical Research: Space Physics*, 115(A9). Retrieved from [https://](https://agupubs.onlinelibrary.wiley.com/doi/abs/10.1029/2010JA015469)
515 agupubs.onlinelibrary.wiley.com/doi/abs/10.1029/2010JA015469 doi:
516 <https://doi.org/10.1029/2010JA015469>
- 517 Brambles, O. J., Lotko, W., Zhang, B., Wiltberger, M., Lyon, J., & Strange-
518 way, R. J. (2011, jun). Magnetosphere sawtooth oscillations induced by
519 ionospheric outflow. *Science (New York, N.Y.)*, 332(6034), 1183–6. doi:
520 10.1126/science.1202869
- 521 Carruthers, G. R., Page, T., & Meier, R. R. (1976, April). Apollo 16 Lyman alpha
522 imagery of the hydrogen geocorona. *Journal of Geophysical Research: Space*
523 *Physics*, 81, 1664-1672. doi: 10.1029/JA081i010p01664
- 524 Chamberlain, J. W. (1963, August). Planetary coronae and atmospheric evapora-
525 tion. *Planet. Space Sci.*, 11, 901-+. doi: 10.1016/0032-0633(63)90122-3
- 526 Chappell, C. R., Moore, T. E., & Waite Jr., J. H. (1987). The ionosphere as a fully
527 adequate source of plasma for the Earth's magnetosphere. *Journal of Geophys-*
528 *ical Research: Space Physics*, 92(A6), 5896-5910. Retrieved from [https://](https://agupubs.onlinelibrary.wiley.com/doi/abs/10.1029/JA092iA06p05896)
529 agupubs.onlinelibrary.wiley.com/doi/abs/10.1029/JA092iA06p05896
530 doi: 10.1029/JA092iA06p05896
- 531 Coley, W. R., Heelis, R. A., & Hairston, M. R. (2003, December). High-latitude
532 plasma outflow as measured by the DMSP spacecraft. *Journal of Geophysical*
533 *Research*, 108(A), 1441.
- 534 Cornwall, J. M. (1977). On the role of charge exchange in generating unstable waves
535 in the ring current. *Journal of Geophysical Research (1896-1977)*, 82(7), 1188-
536 1196. Retrieved from [https://agupubs.onlinelibrary.wiley.com/doi/abs/](https://agupubs.onlinelibrary.wiley.com/doi/abs/10.1029/JA082i007p01188)
537 [10.1029/JA082i007p01188](https://agupubs.onlinelibrary.wiley.com/doi/abs/10.1029/JA082i007p01188) doi: <https://doi.org/10.1029/JA082i007p01188>
- 538 Dandouras, I. (2021). Ion outflow and escape in the terrestrial magnetosphere:
539 Cluster advances. *Journal of Geophysical Research: Space Physics*, 126(10),
540 e2021JA029753. Retrieved from [https://agupubs.onlinelibrary.wiley](https://agupubs.onlinelibrary.wiley.com/doi/abs/10.1029/2021JA029753)
541 [.com/doi/abs/10.1029/2021JA029753](https://agupubs.onlinelibrary.wiley.com/doi/abs/10.1029/2021JA029753) (e2021JA029753 2021JA029753) doi:
542 <https://doi.org/10.1029/2021JA029753>
- 543 Delzanno, G. L., Borovsky, J. E., Henderson, M. G., Resendiz Lira, P. A., Royter-
544 shteyn, V., & Welling, D. T. (2021). The impact of cold electrons and cold
545 ions in magnetospheric physics. *Journal of Atmospheric and Solar-Terrestrial*
546 *Physics*, 220, 105599. Retrieved from [https://www.sciencedirect.com/](https://www.sciencedirect.com/science/article/pii/S1364682621000596)
547 [science/article/pii/S1364682621000596](https://www.sciencedirect.com/science/article/pii/S1364682621000596) doi: [https://doi.org/10.1016/](https://doi.org/10.1016/j.jastp.2021.105599)
548 [j.jastp.2021.105599](https://doi.org/10.1016/j.jastp.2021.105599)
- 549 Denton, M., & Borovsky, J. (2014, 11). Observations and modeling of magnetic
550 flux tube refilling of the plasmasphere at geosynchronous orbit. *Journal of*
551 *Geophysical Research: Space Physics*, 119. doi: 10.1002/2014JA020491
- 552 Fu, S. Y., Wilken, B., Zong, Q. G., & Pu, Z. Y. (2001). Ion composition varia-
553 tions in the inner magnetosphere: Individual and collective storm effects in
554 1991. *Journal of Geophysical Research: Space Physics*, 106(A12), 29683-29704.
555 Retrieved from [https://agupubs.onlinelibrary.wiley.com/doi/abs/](https://agupubs.onlinelibrary.wiley.com/doi/abs/10.1029/2000JA900173)
556 [10.1029/2000JA900173](https://agupubs.onlinelibrary.wiley.com/doi/abs/10.1029/2000JA900173) doi: <https://doi.org/10.1029/2000JA900173>
- 557 Genestreti, K. J., Goldstein, J., Corley, G. D., Farner, W., Kistler, L. M., Larsen,
558 B. A., ... Turner, N. E. (2017). Temperature of the plasmasphere from van
559 allen probes hope. *Journal of Geophysical Research: Space Physics*, 122(1),
560 310-323. Retrieved from [https://agupubs.onlinelibrary.wiley.com/doi/](https://agupubs.onlinelibrary.wiley.com/doi/abs/10.1002/2016JA023047)
561 [abs/10.1002/2016JA023047](https://agupubs.onlinelibrary.wiley.com/doi/abs/10.1002/2016JA023047) doi: <https://doi.org/10.1002/2016JA023047>
- 562 Gershman, D. J., Avakov, L. A., Boardsen, S. A., Dorelli, J. C., Gliese, U., Barrie,
563 A. C., ... Pollock, C. J. (2017). Spacecraft and instrument photoelectrons
564 measured by the dual electron spectrometers on mms. *Journal of Geophysical*
565 *Research: Space Physics*, 122(11), 11,548-11,558. Retrieved from [https://](https://agupubs.onlinelibrary.wiley.com/doi/abs/10.1002/2017JA024518)
566 agupubs.onlinelibrary.wiley.com/doi/abs/10.1002/2017JA024518 doi:

- 567 <https://doi.org/10.1002/2017JA024518>
- 568 Glocer, A., Tóth, G., Gombosi, T., & Welling, D. (2009, May). Modeling iono-
569 spheric outflows and their impact on the magnetosphere, initial results. *Jour-
570 nal of Geophysical Research (Space Physics)*, *114*(A13), 5216-+. doi: 10.1029/
571 2009JA014053
- 572 Haaland, S., Eriksson, A., André, M., Maes, L., Baddeley, L., Barakat, A., ...
573 Welling, D. (2015). Estimation of cold plasma outflow during geomagnetic
574 storms. *Journal of Geophysical Research: Space Physics*, *120*(12), 10,622-
575 10,639. Retrieved from [https://agupubs.onlinelibrary.wiley.com/doi/
576 abs/10.1002/2015JA021810](https://agupubs.onlinelibrary.wiley.com/doi/abs/10.1002/2015JA021810) doi: <https://doi.org/10.1002/2015JA021810>
- 577 Hodges, R. R., Jr. (1994, December). Monte Carlo simulation of the terrestrial hy-
578 drogen exosphere. *Journal of Geophysical Research: Space Physics*, *99*, 23229-
579 +. doi: 10.1029/94JA02183
- 580 Huddleston, M. M., Chappell, C. R., Delcourt, D. C., Moore, T. E., Giles, B. L.,
581 & Chandler, M. O. (2005). An examination of the process and magni-
582 tude of ionospheric plasma supply to the magnetosphere. *Journal of Geo-
583 physical Research: Space Physics*, *110*(A12). Retrieved from [https://
584 agupubs.onlinelibrary.wiley.com/doi/abs/10.1029/2004JA010401](https://agupubs.onlinelibrary.wiley.com/doi/abs/10.1029/2004JA010401) doi:
585 <https://doi.org/10.1029/2004JA010401>
- 586 Hultqvist, B. (1979, June). The hot ion component of the magnetospheric plasma
587 and some relations to the electron component - Observations and physical
588 implications. *Space Science Reviews*, *23*(4), 581-675.
- 589 Hultqvist, B. (1982). Recent progress in the understanding of the ion com-
590 position in the magnetosphere and some major question marks. *Re-
591 views of Geophysics*, *20*(3), 589-611. Retrieved from [https://agupubs
592 .onlinelibrary.wiley.com/doi/abs/10.1029/RG020i003p00589](https://agupubs.onlinelibrary.wiley.com/doi/abs/10.1029/RG020i003p00589) doi:
593 <https://doi.org/10.1029/RG020i003p00589>
- 594 Ilie, R., & Liemohn, M. W. (2016, September). The outflow of ionospheric nitrogen
595 ions: A possible tracer for the altitude-dependent transport and energiza-
596 tion processes of ionospheric plasma. *Journal of Geophysical Research: Space
597 Physics*, *121*(9), 9250-9255.
- 598 Ilie, R., Liemohn, M. W., & Toth, G. (2015). Testing the magnetotail configura-
599 tion based low 2 altitude isotropic boundaries. *Journal of Geophysical Research
600 (Space Physics)*. (2015JA021858) doi: 10.1002/2015JA021858
- 601 Ilie, R., Liemohn, M. W., Toth, G., & Skoug, R. M. (2012). Kinetic model of
602 the inner magnetosphere with arbitrary magnetic field. *Journal of Geo-
603 physical Research: Space Physics*, *117*(A4). Retrieved from [https://
604 agupubs.onlinelibrary.wiley.com/doi/abs/10.1029/2011JA017189](https://agupubs.onlinelibrary.wiley.com/doi/abs/10.1029/2011JA017189) doi:
605 10.1029/2011JA017189
- 606 Ilie, R., Skoug, R., Funsten, H., Liemohn, M., Bailey, J., & Gruntman, M. (2013).
607 The impact of geocoronal density on ring current development. *Journal of At-
608 mospheric and Solar-Terrestrial Physics*, *99*, 92 - 103. Retrieved from [http://
609 www.sciencedirect.com/science/article/pii/S1364682612000946](http://www.sciencedirect.com/science/article/pii/S1364682612000946) (Dy-
610 namics of the Complex Geospace System) doi: [https://doi.org/10.1016/j.jastp
611 .2012.03.010](https://doi.org/10.1016/j.jastp.2012.03.010)
- 612 James, M. K., Yeoman, T. K., Jones, P., Sandhu, J. K., & Goldstein, J. (2021). The
613 scalable plasma ion composition and electron density (spiced) model for earth's
614 inner magnetosphere. *Journal of Geophysical Research: Space Physics*, *126*(9),
615 e2021JA029565. Retrieved from [https://agupubs.onlinelibrary.wiley
616 .com/doi/abs/10.1029/2021JA029565](https://agupubs.onlinelibrary.wiley.com/doi/abs/10.1029/2021JA029565) (e2021JA029565 2021JA029565) doi:
617 <https://doi.org/10.1029/2021JA029565>
- 618 Kistler, L. M., Ipavich, F. M., Hamilton, D. C., Gloeckler, G., Wilken, B., Kremser,
619 G., & Stüdemann, W. (1989). Energy spectra of the major ion species
620 in the ring current during geomagnetic storms. *Journal of Geophysical
621 Research: Space Physics*, *94*(A4), 3579-3599. Retrieved from <https://>

- 622 agupubs.onlinelibrary.wiley.com/doi/abs/10.1029/JA094iA04p03579
623 doi: 10.1029/JA094iA04p03579
- 624 Kistler, L. M., & Mouikis, C. G. (2016, March). The inner magnetosphere ion com-
625 position and local time distribution over a solar cycle. *Journal of Geophysical*
626 *Research: Space Physics*, 121(3), 2009–2032.
- 627 Kozyra, J. U., Liemohn, M. W., Clauer, C. R., Ridley, A. J., Thomsen, M. F.,
628 Borovsky, J. E., ... Gonzalez, W. D. (2002, August). Multistep Dst develop-
629 ment and ring current composition changes during the 4-6 June 1991 magnetic
630 storm. *Journal of Geophysical Research (Space Physics)*, 107, 1224+. doi:
631 10.1029/2001JA000023
- 632 Lee, J. H., Blum, L. W., & Chen, L. (2021). On the impacts of ions of iono-
633 spheric origin and their composition on magnetospheric ionic waves. *Fron-*
634 *tiers in Astronomy and Space Sciences*, 8, 122. Retrieved from [https://](https://www.frontiersin.org/article/10.3389/fspas.2021.719715)
635 www.frontiersin.org/article/10.3389/fspas.2021.719715 doi:
636 10.3389/fspas.2021.719715
- 637 Liemohn, M. W. (2006). Introduction to special section on “results of the na-
638 tional science foundation geospace environment modeling inner magneto-
639 sphere/storms assessment challenge”. *Journal of Geophysical Research:*
640 *Space Physics*, 111(A11). Retrieved from [https://agupubs.onlinelibrary](https://agupubs.onlinelibrary.wiley.com/doi/abs/10.1029/2006JA011970)
641 [.wiley.com/doi/abs/10.1029/2006JA011970](https://agupubs.onlinelibrary.wiley.com/doi/abs/10.1029/2006JA011970) doi: [https://doi.org/10.1029/](https://doi.org/10.1029/2006JA011970)
642 2006JA011970
- 643 Liemohn, M. W., & Kozyra, J. U. (2003, May). Lognormal form of the ring current
644 energy content. *Journal of Atmospheric and Solar-Terrestrial Physics*, 65, 871-
645 886. doi: 10.1016/S1364-6826(03)00088-9
- 646 Liemohn, M. W., & Kozyra, J. U. (2005). Testing the Hypothesis That Charge Ex-
647 change Can Cause a Two-Phase Decay. In T. I. Pulkkinen, N. A. Tsyganenko,
648 & R. H. W. Friedel (Ed.), *The inner magnetosphere: Physics and modeling*
649 (Vol. 155, p. 211+).
- 650 Liemohn, M. W., Kozyra, J. U., Jordanova, V. K., Khazanov, G. V., Thomsen,
651 M. F., & Cayton, T. E. (1999). Analysis of early phase ring current recovery
652 mechanisms during geomagnetic storms. *Geophysical Research Letters*, 26(18),
653 2845-2848. Retrieved from [https://agupubs.onlinelibrary.wiley.com/](https://agupubs.onlinelibrary.wiley.com/doi/abs/10.1029/1999GL900611)
654 [doi/abs/10.1029/1999GL900611](https://agupubs.onlinelibrary.wiley.com/doi/abs/10.1029/1999GL900611) doi: 10.1029/1999GL900611
- 655 Liemohn, M. W., Ridley, A. J., Brandt, P. C., Gallagher, D. L., Kozyra, J. U., Ober,
656 D. M., ... DeMajistre, R. (2005, December). Parametric analysis of nightside
657 conductance effects on inner magnetospheric dynamics for the 17 April 2002
658 storm. *Journal of Geophysical Research (Space Physics)*, 110(A9), 12. doi:
659 10.1029/2005JA011109
- 660 Liemohn, M. W., Ridley, A. J., Gallagher, D. L., Ober, D. M., & Kozyra, J. U.
661 (2004). Dependence of plasmaspheric morphology on the electric field descrip-
662 tion during the recovery phase of the 17 April 2002 magnetic storm. *Journal*
663 *of Geophysical Research: Space Physics*, 109(A3). Retrieved from [https://](https://agupubs.onlinelibrary.wiley.com/doi/abs/10.1029/2003JA010304)
664 agupubs.onlinelibrary.wiley.com/doi/abs/10.1029/2003JA010304 doi:
665 10.1029/2003JA010304
- 666 Moore, T. E., Chappell, C. R., Chandler, M. O., Craven, P. D., Giles, B. L., Pollock,
667 C. J., ... Mozer, F. S. (1997). High-altitude observations of the polar wind.
668 *Science*, 277(5324), 349-351. Retrieved from [https://www.science.org/doi/](https://www.science.org/doi/abs/10.1126/science.277.5324.349)
669 [abs/10.1126/science.277.5324.349](https://www.science.org/doi/abs/10.1126/science.277.5324.349) doi: 10.1126/science.277.5324.349
- 670 Mozer, F., Agapitov, O., Angelopoulos, V., Hull, A., Larson, D., Lejosne, S., &
671 McFadden, J. (2016, 12). Extremely field-aligned cool electrons in the day-
672 side outer magnetosphere: Field-aligned cool electrons. *Geophysical Research*
673 *Letters*, 44. doi: 10.1002/2016GL072054
- 674 Obana, Y., Menk, F. W., & Yoshikawa, I. (2010). Plasma refilling rates for l =
675 2.3–3.8 flux tubes. *Journal of Geophysical Research: Space Physics*, 115(A3).
676 Retrieved from <https://agupubs.onlinelibrary.wiley.com/doi/abs/>

- 677 10.1029/2009JA014191 doi: <https://doi.org/10.1029/2009JA014191>
- 678 Ober, D. M., Horwitz, J. L., & Gallagher, D. L. (1997, July). Formation of density
679 troughs embedded in the outer plasmasphere by subauroral ion drift events.
680 *Journal of Geophysical Research: Space Physics*, *102*, 14595-14602. doi:
681 10.1029/97JA01046
- 682 Orsini, S. (2004). Modeling the time-evolving plasma in the inner magnetosphere:
683 An empirical approach. *Journal of Geophysical Research*, *109*(A11), 18,391.
- 684 Ouellette, J. E., Brambles, O. J., Lyon, J. G., Lotko, W., & Rogers, B. N. (2013).
685 Properties of outflow-driven sawtooth substorms. *Journal of Geophysical Re-*
686 *search: Space Physics*, *118*(6), 3223-3232. Retrieved from [https://agupubs](https://agupubs.onlinelibrary.wiley.com/doi/abs/10.1002/jgra.50309)
687 [.onlinelibrary.wiley.com/doi/abs/10.1002/jgra.50309](https://agupubs.onlinelibrary.wiley.com/doi/abs/10.1002/jgra.50309) doi: [https://doi](https://doi.org/10.1002/jgra.50309)
688 [.org/10.1002/jgra.50309](https://doi.org/10.1002/jgra.50309)
- 689 Phaneuf, R. A., Janev, R. K., & Pindzola, M. S. (1987). *Collisions of carbon and*
690 *oxygen ions with electrons, H, H2 and He*. Springfield.
- 691 Rairden, R. L., Frank, L. A., & Craven, J. D. (1986, December). Geocoronal imag-
692 ing with Dynamics Explorer. *Journal of Geophysical Research: Space Physics*,
693 *91*, 13613-13630. doi: 10.1029/JA091iA12p13613
- 694 Rapp, D., & Francis, W. E. (1962). Charge exchange between gaseous ions and
695 atoms. *The Journal of Chemical Physics*, *37*(11), 2631-2645. Retrieved from
696 <https://doi.org/10.1063/1.1733066> doi: 10.1063/1.1733066
- 697 Smith, P. H., & Bewtra, N. K. (1978, March). Charge exchange lifetimes for ring
698 current ions. *Space Science Reviews*, *22*, 301-318. doi: 10.1007/BF00239804
- 699 Sojka, J. J., & Wrenn, G. L. (1985). Refilling of geosynchronous flux tubes
700 as observed at the equator by geos 2. *Journal of Geophysical Research:*
701 *Space Physics*, *90*(A7), 6379-6385. Retrieved from [https://agupubs](https://agupubs.onlinelibrary.wiley.com/doi/abs/10.1029/JA090iA07p06379)
702 [.onlinelibrary.wiley.com/doi/abs/10.1029/JA090iA07p06379](https://agupubs.onlinelibrary.wiley.com/doi/abs/10.1029/JA090iA07p06379) doi:
703 <https://doi.org/10.1029/JA090iA07p06379>
- 704 Stern, D. P. (1975). The motion of a proton in the equatorial magnetosphere.
705 *Journal of Geophysical Research (1896-1977)*, *80*(4), 595-599. Retrieved
706 from [https://agupubs.onlinelibrary.wiley.com/doi/abs/10.1029/](https://agupubs.onlinelibrary.wiley.com/doi/abs/10.1029/JA080i004p00595)
707 [JA080i004p00595](https://agupubs.onlinelibrary.wiley.com/doi/abs/10.1029/JA080i004p00595) doi: 10.1029/JA080i004p00595
- 708 Su, Y.-J., Thomsen, M. F., Borovsky, J. E., & Lawrence, D. J. (2001). A com-
709 prehensive survey of plasmasphere refilling at geosynchronous orbit. *Journal*
710 *of Geophysical Research: Space Physics*, *106*(A11), 25615-25629. Retrieved
711 from [https://agupubs.onlinelibrary.wiley.com/doi/abs/10.1029/](https://agupubs.onlinelibrary.wiley.com/doi/abs/10.1029/2000JA000441)
712 [2000JA000441](https://agupubs.onlinelibrary.wiley.com/doi/abs/10.1029/2000JA000441) doi: <https://doi.org/10.1029/2000JA000441>
- 713 Thomsen, M. F., Denton, M. H., Gary, S. P., Liu, K., & Min, K. (2017, December).
714 Ring/Shell Ion Distributions at Geosynchronous Orbit. *Journal of Geophysical*
715 *Research: Space Physics*, *122*(1), 12-.
- 716 Thomsen, M. F., Denton, M. H., Jordanova, V. K., Chen, L., & Thorne, R. M.
717 (2011). Free energy to drive equatorial magnetosonic wave instability at
718 geosynchronous orbit. *Journal of Geophysical Research: Space Physics*,
719 *116*(A8). Retrieved from [https://agupubs.onlinelibrary.wiley.com/doi/](https://agupubs.onlinelibrary.wiley.com/doi/abs/10.1029/2011JA016644)
720 [abs/10.1029/2011JA016644](https://agupubs.onlinelibrary.wiley.com/doi/abs/10.1029/2011JA016644) doi: <https://doi.org/10.1029/2011JA016644>
- 721 Trung, H.-S., Liemohn, M. W., & Ilie, R. (2019). Steady state characteristics of
722 the terrestrial geopauses. *Journal of Geophysical Research: Space Physics*,
723 *124*(7), 5070-5081. Retrieved from [https://agupubs.onlinelibrary.wiley](https://agupubs.onlinelibrary.wiley.com/doi/abs/10.1029/2019JA026636)
724 [.com/doi/abs/10.1029/2019JA026636](https://agupubs.onlinelibrary.wiley.com/doi/abs/10.1029/2019JA026636) doi: [https://doi.org/10.1029/](https://doi.org/10.1029/2019JA026636)
725 [2019JA026636](https://doi.org/10.1029/2019JA026636)
- 726 Volland, H. (1973). A semiempirical model of large-scale magnetospheric elec-
727 tric fields. *Journal of Geophysical Research (1896-1977)*, *78*(1), 171-180.
728 Retrieved from [https://agupubs.onlinelibrary.wiley.com/doi/abs/](https://agupubs.onlinelibrary.wiley.com/doi/abs/10.1029/JA078i001p00171)
729 [10.1029/JA078i001p00171](https://agupubs.onlinelibrary.wiley.com/doi/abs/10.1029/JA078i001p00171) doi: 10.1029/JA078i001p00171
- 730 Welling, D. T., André, M., Dandouras, I., Delcourt, D., Fazakerley, A., Fontaine,
731 D., ... Yau, A. (2015, oct). The Earth: Plasma Sources, Losses, and

- 732 Transport Processes. *Space Science Reviews*, 192(1-4), 145–208. Retrieved
 733 from <http://link.springer.com/10.1007/s11214-015-0187-2> doi:
 734 10.1007/s11214-015-0187-2
- 735 Welling, D. T., Jordanova, V. K., Glocer, A., Toth, G., Liemohn, M. W., & Weimer,
 736 D. R. (2015, jun). The two-way relationship between ionospheric outflow and
 737 the ring current. *Journal of Geophysical Research: Space Physics*, 120(6),
 738 4338–4353. Retrieved from <http://doi.wiley.com/10.1002/2015JA021231>
 739 doi: 10.1002/2015JA021231
- 740 Welling, D. T., & Ridley, A. J. (2010, April). Exploring sources of magnetospheric
 741 plasma using multispecies MHD. *Journal of Geophysical Research*, 115(A),
 742 A04201.
- 743 Wiltberger, M., Lotko, W., Lyon, J. G., Damiano, P., & Merkin, V. (2010, Octo-
 744 ber). Influence of cusp O⁺ outflow on magnetotail dynamics in a multifluid
 745 MHD model of the magnetosphere. *Journal of Geophysical Research*, 115(1),
 746 A00J05.
- 747 Winglee, R. M. (2000). Mapping of ionospheric outflows into the magnetosphere for
 748 varying IMF conditions. *Journal of Atmospheric and Solar-Terrestrial Physics*,
 749 62, 527–540. Retrieved from [http://www.sciencedirect.com/science/
 750 article/pii/S1364682600000158](http://www.sciencedirect.com/science/article/pii/S1364682600000158)
- 751 Winglee, R. M., Chua, D., Brittnacher, M., Parks, G. K., & Lu, G. (2002, Septem-
 752 ber). Global impact of ionospheric outflows on the dynamics of the magneto-
 753 sphere and cross-polar cap potential. *Journal of Geophysical Research (Space
 754 Physics)*, 107, 1237. doi: 10.1029/2001JA000214
- 755 Young, D. T., Balsiger, H., & Geiss, J. (1982). Correlations of magnetospheric
 756 ion composition with geomagnetic and solar activity. *Journal of Geophysi-
 757 cal Research: Space Physics*, 87(A11), 9077-9096. Retrieved from [https://
 758 agupubs.onlinelibrary.wiley.com/doi/abs/10.1029/JA087iA11p09077](https://agupubs.onlinelibrary.wiley.com/doi/abs/10.1029/JA087iA11p09077)
 759 doi: 10.1029/JA087iA11p09077
- 760 Yu, Y., Liemohn, M. W., Jordanova, V. K., Lemon, C., & Zhang, J. (2019). Re-
 761 cent advancements and remaining challenges associated with inner magneto-
 762 sphere cross-energy/population interactions (imcepi). *Journal of Geophys-
 763 ical Research: Space Physics*, 124(2), 886-897. Retrieved from [https://
 764 agupubs.onlinelibrary.wiley.com/doi/abs/10.1029/2018JA026282](https://agupubs.onlinelibrary.wiley.com/doi/abs/10.1029/2018JA026282) doi:
 765 <https://doi.org/10.1029/2018JA026282>
- 766 Zhao, H., Li, X., Baker, D. N., Fennell, J. F., Blake, J. B., Larsen, B. A., ... Ro-
 767 driguez, J. V. (2015). The evolution of ring current ion energy density and
 768 energy content during geomagnetic storms based on Van Allen Probes mea-
 769 surements. *Journal of Geophysical Research: Space Physics*, 120(9), 7493–
 770 7511. Retrieved from <http://dx.doi.org/10.1002/2015JA021533> doi:
 771 10.1002/2015JA021533
- 772 Zoennchen, J. H., Bailey, J. J., Nass, U., Gruntman, M., Fahr, H. J., & Goldstein,
 773 J. (2011, July). 3-D-geocoronal hydrogen density derived from TWINS Ly- α -
 774 data. *Annales Geophysicae*, 13.
- 775 Zoennchen, J. H., Connor, H. K., Jung, J., Nass, U., & Fahr, H. J. (2022). Ter-
 776 restrial exospheric dayside h-density profile at 3–15 r_E from uvis/hdac and
 777 twins lyman- α data combined. *Annales Geophysicae*, 40(3), 271–279. Re-
 778 trieved from <https://angeo.copernicus.org/articles/40/271/2022/> doi:
 779 10.5194/angeo-40-271-2022
- 780 Zoennchen, J. H., Nass, U., & Fahr, H. J. (2015). Terrestrial exospheric hydrogen
 781 density distributions under solar minimum and solar maximum conditions
 782 observed by the twins stereo mission. *Annales Geophysicae*, 33(3), 413–426.
 783 Retrieved from <https://angeo.copernicus.org/articles/33/413/2015/>
 784 doi: 10.5194/angeo-33-413-2015